

Study for (anti)hypertriton and light (anti)nuclei production in high energy collisions at $\sqrt{S_{NN}} = 200$ GeV

Hai-Jun Li*, Ting-Ting Zeng, Gang Chen
*School of Mathematics and Physics,
 China University of Geosciences,
 Wuhan 430074, P. R. China*

We used the parton and hadron cascade (PACIAE) model and the dynamically constrained phase-space coalescence (DCPC) model to investigate the production of (anti)hypertriton and light (anti)nuclei generated by 0-10% centrality $^{12}\text{C}+^{12}\text{C}$, $^{24}\text{Mg}+^{24}\text{Mg}$, $^{40}\text{Ca}+^{40}\text{Ca}$ and $^{64}\text{Cu}+^{64}\text{Cu}$ collisions at $\sqrt{S_{NN}} = 200$ GeV with $|y| < 1.5$ and $p_T < 5$. We studied the yield ratios of antiparticle to particle and the rapidity distributions of the different (anti)nuclei, and found that the amount of antimatter produced is significantly lower than that of the corresponding particles, the results of theoretical model are well consistent with PHOBOS data. The yield ratios of the particle to antiparticle in different transverse momentum region is also given, and we found the ratios is increased with the increase of the transverse momentum.

I. INTRODUCTION

In 1928, Dirac predicted the existence of negative energy states (i.e., antimatter) of electrons depending on the symmetry principle of quantum mechanics for the first time [1]. According to the Big Bang theory [2], it is generally accepted that equal amounts of matter and antimatter have been produced during the initial stage of the universe. However, this symmetry got lost in a series of evolution of the universe with no significant amount of antimatter being present [3]. Because the high energy heavy-ion collisions create abundant hyperons and nucleons, and the initial fireball produced in ultrarelativistic heavy-ion collisions is similar to the initial stage of the universe, so the study of antinuclei production in ultrarelativistic heavy-ion collisions maybe a better choice to solve above puzzle [4]. However, because of the low abundance, the study of light nuclei (antinuclei) production is quite difficult both experimentally and theoretically [5].

The antimatter nuclei have been widely studied in cosmic ray [6, 7] and detected at the accelerator experiment [8, 9] could be an indirect signal of the new physics, such as dark matter and the study of manmade matter called quark gluon plasma (QGP) [10, 11], respectively. Hypernuclei provide a doorway to the production of strangelets, and a unique opportunity to study the hyperon-nucleon (YN) and hyperon-hyperon (YY) interactions [12]. The measurements of YN and YY interactions are essential for the theoretical study of neutron stars [13] and exotic states of finite nuclei [14]. In 2010, the STAR Collaboration has reported their measurements of $^3_\Lambda H$ and $^3_{\bar{\Lambda}}\bar{H}$ production in Au+Au collisions at top Relativistic Heavy-Ion Collider (RHIC) energy [15]. They have measured 70 ± 17 antihypertritons ($^3_{\bar{\Lambda}}\bar{H}$) and 157 ± 30 hypertritons ($^3_\Lambda H$) in the 89×10^6 minimum-bias and 22×10^6 central (head-on) Au+Au collision events. And in total $18 \text{ } ^4\text{He}$ counts were detected at the STAR experiment at RHIC in 10^9 recorded Au+Au collisions at center-of-mass energies of 200 GeV and 62 GeV per nucleon-nucleon pair in 2011 [16]. Therefore, we have a simulation study about the production of (anti)hypertriton and light (anti)nuclei at high energy (200 GeV) in $^{12}\text{C}+^{12}\text{C}$, $^{24}\text{Mg}+^{24}\text{Mg}$, $^{40}\text{Ca}+^{40}\text{Ca}$ and $^{64}\text{Cu}+^{64}\text{Cu}$ collisions.

We have proposed a dynamically constrained phase-space coalescence (DCPC) model [17] based on the PACIAE [18, 19]. Then we have predicted the light nuclei (antinuclei) yield, transverse momentum distributions and the rapidity distributions in pp collisions at 7 and 14 TeV [17]. And we have investigated the light nuclei (antinuclei), hypernuclei (antihypernuclei) productions [5] and their centrality dependence [20], scaling feature [21] in the 0-5% most central Au+Au collisions at 200 GeV. So these make the study for the (anti)hypertriton and light (anti)nuclei production in nucleon-nucleon (NN) collisions possible.

This paper is organized as follows: In Sec. II, the PACIAE model coupled with the DCPC model is developed to study the production rates of hypertriton ($^3_\Lambda H$) and light nuclei, i.e. d , t , and ^3He to corresponding their antimatter with $^{12}\text{C}+^{12}\text{C}$, $^{24}\text{Mg}+^{24}\text{Mg}$, $^{40}\text{Ca}+^{40}\text{Ca}$ and $^{64}\text{Cu}+^{64}\text{Cu}$ beams of energy at $\sqrt{S_{NN}} = 200$ GeV. In Sec. III, we calculated the yield ratios of antiparticle to particle in $^{12}\text{C}+^{12}\text{C}$, $^{24}\text{Mg}+^{24}\text{Mg}$, $^{40}\text{Ca}+^{40}\text{Ca}$ and $^{64}\text{Cu}+^{64}\text{Cu}$ collisions, the study of rapidity distributions and transverse momentum distributions of \bar{d}/d , \bar{t}/t , $^3\bar{\text{He}}/^3\text{He}$ and $^3_{\bar{\Lambda}}\bar{H}/^3_\Lambda H$ is also given. And a short summary is the content of Sec. IV.

* Corresponding Author: lhj718@foxmail.com

II. MODELS

The PYTHIA model (PYTHIA 6.4 [22]) is devised for high-energy hadron-hadron collisions. In this model, a hadron-hadron collision is decomposed into parton-parton collisions. The hard parton-parton scattering is described by the leading-order perturbative QCD (Lo-pQCD) parton-parton interactions with the modification of parton distribution function in a hadron. The soft parton-parton collision, a nonperturbative phenomenon, is considered empirically. The initial- and final-state QCD radiations and the multiparton interactions are also taken into account. Therefore, the consequence of a hadron-hadron collision is a partonic multijet state composed of diquarks (antidiquarks), quarks (antiquarks) and gluons, as well as a few hadronic remnants. This is then followed by string construction and fragmentation. A hadronic final state is eventually obtained for a hadron-hadron collision.

The parton and hadron cascade PACIAE [18, 19] model is based on PYTHIA 6.4 and is mainly devised for nucleus-nucleus collisions. In the PACIAE model, first the nucleus-nucleus collision is decomposed into nucleon-nucleon (NN) collisions according to the collision geometry and NN total cross section. Each NN collision is described by the PYTHIA model with the string fragmentation switches-off and the diquarks (antidiquarks) randomly breaks into quarks (antiquarks). So the consequence of a NN collision is now a partonic initial state composed of quarks, antiquarks and gluons. Provided all NN collisions are exhausted, one obtains a partonic initial state for a nucleus-nucleus collision. This partonic initial state is regarded as the quark-gluon matter (QGM) formed in relativistic nucleus-nucleus collisions. Second, the parton rescattering proceeds. The rescattering among partons in QGM is randomly considered by the $2 \rightarrow 2$ Lo-pQCD parton-parton cross sections [23]. In addition, a K factor is introduced here to include the higher order and the nonperturbative corrections. Third, hadronization follows after parton rescattering. The partonic matter can be hadronized by the Lund string fragmentation regime [22] and/or the phenomenological coalescence model [19]. Finally, the hadronic matter proceeds to rescatter until hadronic freeze-out (the exhaustion of the hadron-hadron collision pairs [24, 25]). We refer to Ref. [19] for the details.

In quantum statistical mechanics [26, 27], one cannot precisely define both position $\vec{q} \equiv (x, y, z)$ and momentum $\vec{p} \equiv (p_x, p_y, p_z)$ of a particle in the six-dimension phase space because of the uncertainty principle

$$\Delta \vec{q} \Delta \vec{p} \sim h^3. \quad (1)$$

We can only say that this particle lies somewhere within a six-dimension quantum “box” or “state” with the volume of $\Delta \vec{q} \Delta \vec{p}$. A particle state occupies a volume of h^3 in the six-dimension phase space [26, 27]. Therefore one can estimate the yield of a single particle by

$$\int_{H \leq E} \frac{d\vec{q} d\vec{p}}{h^3}. \quad (2)$$

where H and E are the Hamiltonian and energy of the particle, respectively. Similarly, the yield of N -particle cluster can be estimated by

$$\int \dots \int_{H \leq E} \frac{d\vec{q}_1 d\vec{p}_1 \dots d\vec{q}_N d\vec{p}_N}{h^{3N}}. \quad (3)$$

Therefore the yield of $\frac{3}{\Lambda} \overline{H}$ in our dynamically constrained phase-space coalescence model, for instance, is assumed to be

$$y = \int \dots \int \delta_{123} \frac{d\vec{q}_1 d\vec{p}_1 d\vec{q}_2 d\vec{p}_2 d\vec{q}_3 d\vec{p}_3}{h^9}, \quad (4)$$

$$\delta_{123} = \begin{cases} 1 & \text{if } 1 \equiv \bar{p}, \ 2 \equiv \bar{n}, \ 3 \equiv \bar{\Lambda}, \text{ and combination;} \\ & m_0 \leq m_{inv} \leq m_0 + \Delta m; \\ & |\vec{q}_{12}| \leq D_0, \ |\vec{q}_{13}| \leq D_0, \ |\vec{q}_{23}| \leq D_0; \\ 0 & \text{otherwise;} \end{cases} \quad (5)$$

where

$$m_{inv} = [(E_1 + E_2 + E_3)^2 - (\vec{p}_1 + \vec{p}_2 + \vec{p}_3)^2]^{1/2}, \quad (6)$$

here (E_1, E_2, E_3) and $(\vec{p}_1, \vec{p}_2, \vec{p}_3)$ are the energy and momentum of particles \bar{p} , \bar{n} and $\bar{\Lambda}$, respectively. In Eq. (5), m_0 and D_0 stand for, respectively, the rest mass and diameter of $\frac{3}{\Lambda} \overline{H}$, Δm refers to the allowed mass uncertainty, and $|\vec{q}_{ij}| = |\vec{q}_i - \vec{q}_j|$ is the vector distance between particles i and j .

As the hadron position and momentum distributions from transport model simulations are discrete, the integral over continuous distributions in Eq. (5) should be replaced by the sum over discrete distributions. In a single event

TABLE I: The integrated yield dN/dy of particles with 0-10% centrality, for p , \bar{p} , Λ and $\bar{\Lambda}$ in $^{64}\text{Cu}+^{64}\text{Cu}$ collisions at $\sqrt{S_{NN}} = 62.4$ GeV and $\sqrt{S_{NN}} = 200$ GeV.

Particle type	62.4(GeV)		200(GeV)	
	PACIAE	PHENIX ^a	PACIAE	STAR ^b
p	4.49	4.54	7.48	
\bar{p}	2.57	2.73	4.82	
Λ	2.18		4.75	4.68 ± 0.45
$\bar{\Lambda}$	1.45		3.58	3.79 ± 0.37

^a The PHENIX data are taken from Ref. [28]

^b The STAR data are taken from Ref. [29]

of the final hadronic state obtained from transport model simulation, the configuration of the $\frac{3}{\Lambda}H$ ($\bar{p}+\bar{n}+\bar{\Lambda}$) system can be expressed as

$$C_{\bar{p}\bar{n}\bar{\Lambda}}(\Delta q_1, \Delta q_2, \Delta q_3; \vec{p}_1, \vec{p}_2, \vec{p}_3), \quad (7)$$

where the subscripts $1 \equiv \bar{p}$, $2 \equiv \bar{n}$, $3 \equiv \bar{\Lambda}$, and q_1 refers to the distance between \bar{p} and the center-of-mass of \bar{p} , \bar{n} , and $\bar{\Lambda}$ for instance. Then the third constraint (diameter constraint) in Eq. (5) is correspondingly replaced by

$$\Delta q_1 \leq R_0, \quad \Delta q_2 \leq R_0, \quad \Delta q_3 \leq R_0, \quad (8)$$

where R_0 refers to the radius of $\frac{3}{\Lambda}H$.

Each of the above configurations contributes a partial yield of

$$y_{123} = \begin{cases} 1 & \text{if } m_0 \leq m_{inv} \leq m_0 + \Delta m, \\ & \Delta q_1 \leq R_0, \Delta q_2 \leq R_0, \Delta q_3 \leq R_0; \\ 0 & \text{otherwise;} \end{cases} \quad (9)$$

to the yield of $\frac{3}{\Lambda}H$. So the total yield of $\frac{3}{\Lambda}H$ in a single event is the sum of the above partial yield over the configurations of Eq. (7) and their combinations. An average over events is required at the end.

III. RESULTS AND DISCUSSION

First we produce the final state particles using the PACIAE [18, 19] model. In the PACIAE simulations, we assume that hyperons are heavier than Λ decay already. The model parameters are fixed on the default values given in PYTHIA model. However, the K factor as well as the parameters $\text{parj}(1)$, $\text{parj}(2)$ and $\text{parj}(3)$, relevant to the strange production in PYTHIA, are given by fitting the PHENIX data of p , \bar{p} in Cu+Cu collisions at $\sqrt{S_{NN}} = 62.4$ GeV by the 0-10% centrality with $3.0 < |y| < 3.9$ and $0.5 < p_T < 4.5$ [28] and the STAR data of Λ , $\bar{\Lambda}$ in Cu+Cu collisions at $\sqrt{S_{NN}} = 200$ GeV by the 0-10% centrality with $|y| < 0.5$ and $p_T < 5$ [29], as shown in Tab. I. The fitted parameters of $K = 3$ (default value is 1 or 1.5), $\text{parj}(1) = 0.15$ (0.1), $\text{parj}(2) = 0.45$ (0.3) and $\text{parj}(3) = 0.65$ (0.4). And the yields dN/dy of \bar{d} is calculated by the DCPC model in Cu+Cu collisions at $\sqrt{S_{NN}} = 200$ GeV by 0-10% centrality with $|y| < 0.9$ and $0.2 < p_T < 0.9$, we calculated the $\Delta m = 0.0003$, the results from our model agree well with the experimental data from STAR [30].

Then, we generate 5×10^7 minimum-bias events by the PACIAE model in $^{12}\text{C}+^{12}\text{C}$, $^{24}\text{Mg}+^{24}\text{Mg}$, $^{40}\text{Ca}+^{40}\text{Ca}$ and $^{64}\text{Cu}+^{64}\text{Cu}$ collisions at $\sqrt{S_{NN}} = 200$ GeV, the rapidity region we selected is $|y| < 1.5$, and the transverse momentum region is $0 < p_T < 5$ (GeV/c). The integrated yields dN/dy of (anti)hypertriton $\frac{3}{\Lambda}H$ ($\frac{3}{\Lambda}\bar{H}$) and light (anti)nuclei d (\bar{d}), t (\bar{t}) as well as ^3He ($\bar{^3\text{He}}$) are calculated by the DCPC model, as shown in Tab. II.

TABLE II: The integrated yield dN/dy of particles at midrapidity ($|y| < 0.5$) with 0-10% centrality, for d (\bar{d}), t (\bar{t}), 3He ($\overline{{}^3He}$) and ${}^3_\Lambda H$ ($\overline{{}^3_\Lambda H}$) in ${}^{12}C+{}^{12}C$, ${}^{24}Mg+{}^{24}Mg$, ${}^{40}Ca+{}^{40}Ca$ and ${}^{64}Cu+{}^{64}Cu$ collisions at $\sqrt{S_{NN}} = 200$ GeV.

Collision types	d	\bar{d}	t	\bar{t}	3He	$\overline{{}^3He}$	${}^3_\Lambda H$	$\overline{{}^3_\Lambda H}$
${}^{12}C+{}^{12}C$	2.187E-03	1.415E-03	4.227E-07	2.292E-07	3.492E-07	1.721E-07	2.364E-07	1.104E-07
${}^{24}Mg+{}^{24}Mg$	7.301E-03	4.598E-03	1.114E-06	5.907E-07	9.121E-07	4.455E-07	6.453E-07	2.942E-07
${}^{40}Ca+{}^{40}Ca$	2.094E-02	1.298E-02	2.676E-06	1.391E-06	2.189E-06	1.048E-06	1.722E-06	7.629E-07
${}^{64}Cu+{}^{64}Cu$	3.835E-02	2.397E-02	4.181E-06	2.163E-06	3.731E-06	1.780E-06	2.783E-06	1.207E-06

In FIG. 1, The yield ratios of antiparticle to particle are given, π^-/π^+ , K^-/K^+ , \bar{p}/p , \bar{n}/n , $\bar{\Lambda}/\Lambda$, $\overline{\Xi^-}/\Xi^-$ and $\overline{\Omega^-}/\Omega^-$. For the different collision nucleon, ${}^{12}C+{}^{12}C$, ${}^{24}Mg+{}^{24}Mg$, ${}^{40}Ca+{}^{40}Ca$ and ${}^{64}Cu+{}^{64}Cu$, the ratios of antiparticle to particle are roughly unchanged. And we found that the bigger the nucleon number of the collisions nucleon is, the lower the yield ratios of antiparticles to particles is. It means that the production of antimatter in the collisions of light nuclei is easier in the same conditions, and this is both for nucleus and particles production. We also can see that the particles (π^+ , K^+ , p , n , Λ , Ξ^- and Ω^-) ratios approach to 1 while the hypertriton (${}^3_\Lambda H$) and light nuclei (d , t and 3He) is less than 1. The results obtained from our model are in agreement with the experimental data from PHOBOS [31].

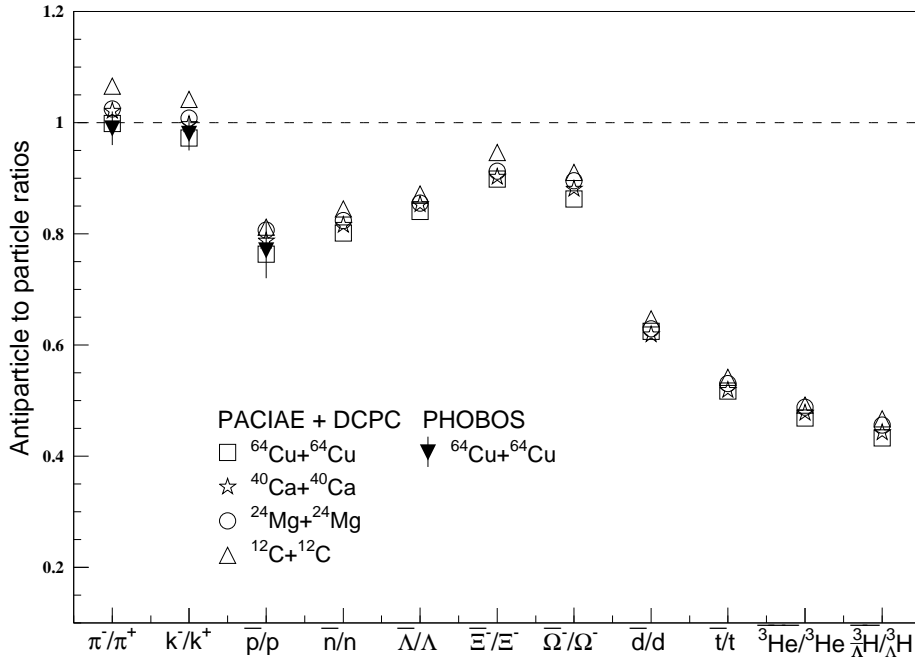


FIG. 1: The yield ratios of particles (π^+ , K^+ , p , n , Λ , Ξ^- , Ω^-) to corresponding antiparticles (π^- , K^- , \bar{p} , \bar{n} , $\bar{\Lambda}$, $\overline{\Xi^-}$, $\overline{\Omega^-}$) in 0-10% centrality ${}^{12}C+{}^{12}C$, ${}^{24}Mg+{}^{24}Mg$, ${}^{40}Ca+{}^{40}Ca$ and ${}^{64}Cu+{}^{64}Cu$ at $\sqrt{S_{NN}} = 200$ GeV reaction. Solid symbols are the experimental data points from PHOBOS [31]. Open symbols represent our PACIAE + DCPC model results.

FIG. 2 shows the rapidity distributions of d , t , 3He , ${}^3_\Lambda H$ and their antinuclei in ${}^{12}C+{}^{12}C$, ${}^{24}Mg+{}^{24}Mg$, ${}^{40}Ca+{}^{40}Ca$ and ${}^{64}Cu+{}^{64}Cu$ collisions at $\sqrt{S_{NN}} = 200$ GeV from PACIAE + DCPC model. The particles and the antiparticles are mainly produced at the mid-rapidity and quickly decrease towards forward (backward) rapidity. It is obviously that the rapidity distributions of antimatter is less than their corresponding matter with the same nucleus collisions. For the same particles produced, and we found that the rapidity distributions increased with the nucleon number of the collision nucleus.

Then we compared the relationship between the nucleon number of the particles produced and their rapidity distributions in the same condition. We found the rapidity distributions for d is different from those for t , 3He and

${}^3_{\Lambda}H$, their rapidity distributions are less than d (a). Because d (a) has two nuclei while t (b), 3He (c) and ${}^3_{\Lambda}H$ (d) all have three nuclei. For the same nucleon number nuclei, t (b) and 3He (c), the former is consists of one proton and two neutron while the latter is consists of two proton and one neutron, we found that the rapidity distributions of t (b) are roughly consistent with the 3He (c), but the former is a little bit higher than the latter. Finally, we compared the t (b) (one proton and two neutron) with the ${}^3_{\Lambda}H$ (d) (one proton, one neutron and one Λ), we found that the rapidity distributions of the particle which has (anti-)hyperon is lower than that replaced by a neutron.

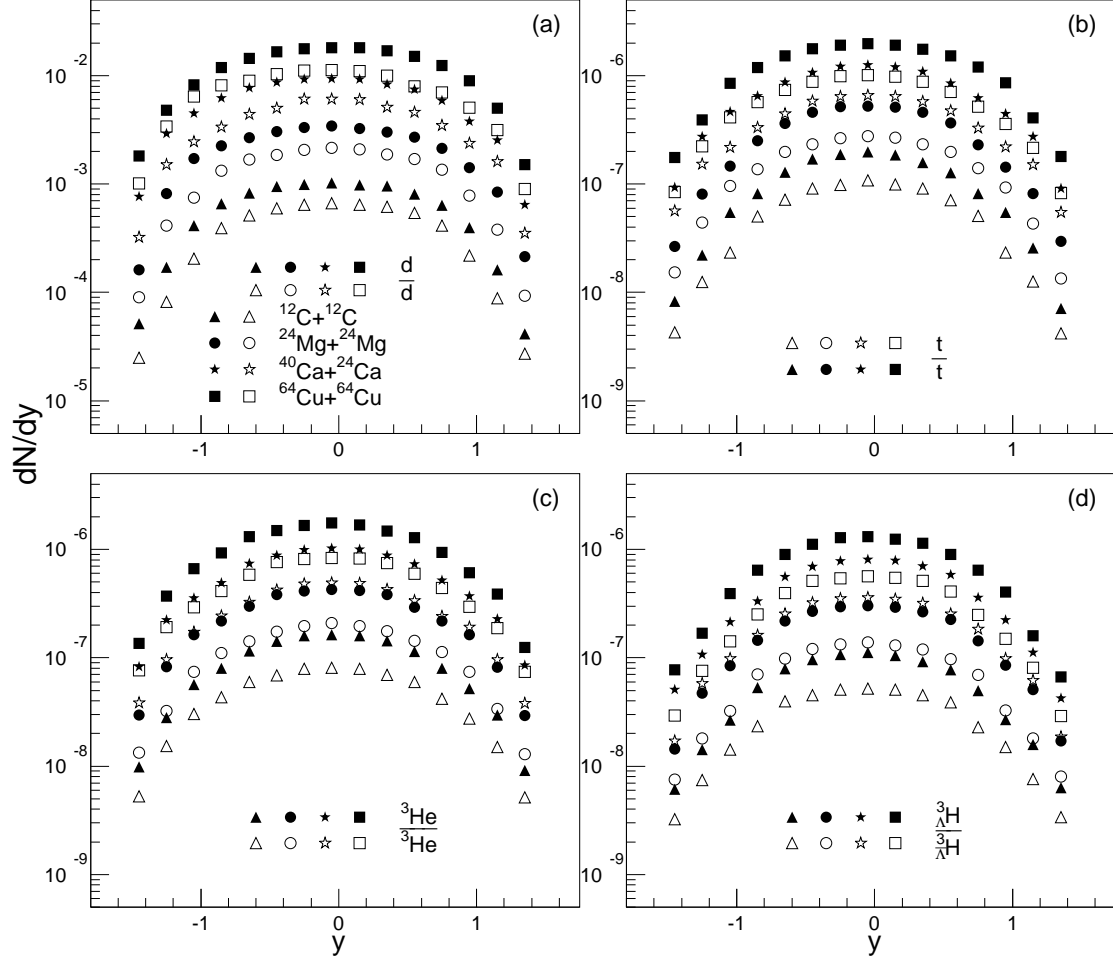


FIG. 2: The rapidity ($|y| < 1.5$) distributions of particles d (a), t (b), 3He (c), and ${}^3_{\Lambda}H$ (d) to corresponding antiparticles \bar{d} (a), \bar{t} (b), $\overline{{}^3He}$ (c), and $\overline{{}^3_{\Lambda}H}$ (d) produced by PACIAE + DCPC model at $\sqrt{S_{NN}} = 200$ GeV in 0-10% centrality ${}^{12}C+{}^{12}C$, ${}^{24}Mg+{}^{24}Mg$, ${}^{40}Ca+{}^{40}Ca$ and ${}^{64}Cu+{}^{64}Cu$ collisions.

The transverse momentum distributions of the ratios for d , t , 3He , ${}^3_{\Lambda}H$ to their antiparticles produced in ${}^{12}C+{}^{12}C$, ${}^{24}Mg+{}^{24}Mg$, ${}^{40}Ca+{}^{40}Ca$ and ${}^{64}Cu+{}^{64}Cu$ collisions is given in FIG. 3. We found that in the same condition, the nucleon number and the particles produced, the ratios of the antiparticle to particle are small at the low transverse momentum region while it have a rapidly increase at the high transverse momentum region. And we also found that under the same transverse momentum, the ratios is inversely proportional to the nucleon number of the collision nucleus.

Then we also compared the relationship between the nucleon number of the particles produced and their antiparticle to particle ratios in the same condition. We found the ratios of \bar{d}/d (a) is higher than that of \bar{t}/t (b), $\overline{{}^3He}/{}^3He$ (c) and $\overline{{}^3_{\Lambda}H}/{}^3_{\Lambda}H$ (d), because of the two nuclei d , and the others are three. For the same nucleon number nuclei, the antiparticle to particle ratios of \bar{t}/t (b), $\overline{{}^3He}/{}^3He$ (c) and $\overline{{}^3_{\Lambda}H}/{}^3_{\Lambda}H$ (d) have a similar distributions.

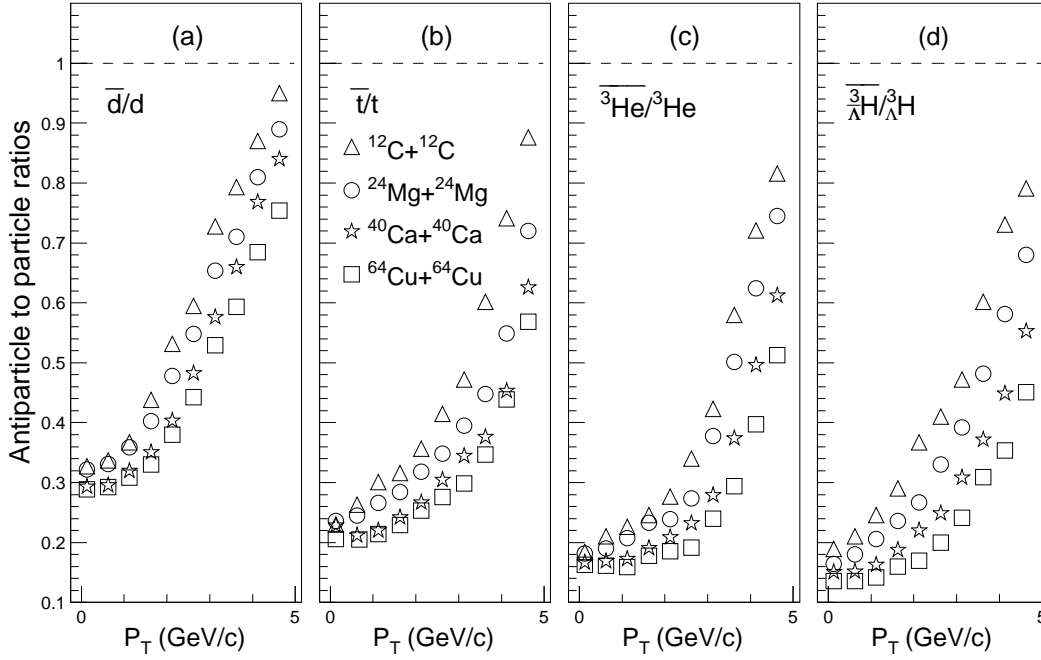


FIG. 3: The p_T dependence of the ratios for antiparticles (\bar{d} , \bar{t} , $\bar{{}^3\text{He}}$, and $\bar{{}^3\text{H}}$) to particles (d , t , ${}^3\text{He}$, and ${}^3\text{H}$) produced by PACIAE + DCPC model at $\sqrt{S_{NN}} = 200$ GeV in 0-10% centrality ${}^{12}\text{C}+{}^{12}\text{C}$, ${}^{24}\text{Mg}+{}^{24}\text{Mg}$, ${}^{40}\text{Ca}+{}^{40}\text{Ca}$ and ${}^{64}\text{Cu}+{}^{64}\text{Cu}$ collisions. The transverse momentum range is 0-5 GeV/c.

IV. CONCLUSION

In this paper, we used the PACIAE + DCPC model to investigate the production of (anti)hypertriton and light (anti)nuclei generated by 0-10% central ${}^{12}\text{C}+{}^{12}\text{C}$, ${}^{24}\text{Mg}+{}^{24}\text{Mg}$, ${}^{40}\text{Ca}+{}^{40}\text{Ca}$ and ${}^{64}\text{Cu}+{}^{64}\text{Cu}$ collisions at $\sqrt{S_{NN}} = 200$ GeV with $|y| < 1.5$ and $p_T < 5$. We studied the yield ratios of antiparticle to particle and the rapidity distributions of the different (anti)nuclei. The results obtained from our model are in agreement with the experimental data from PHOBOS, and it is obviously that the rapidity distributions of antimatter is less than their corresponding matter with the same nucleus collisions. The yield ratios of the particles in different transverse momentum region is also given. We found the ratios is increased with the increase of the transverse momentum, the ratios of the antiparticle to particle are small at the low transverse momentum region while it have a rapidly increase at the high transverse momentum region.

ACKNOWLEDGMENT

Finally, we acknowledge the financial support from SPIE (201310491051) in China.

-
- [1] P. A. M. Dirac, Proc. R. Soc. Lond. A. **117** (1928) 610.
 - [2] G. Gamow, Phys. Rev. **70** (1946) 572.
 - [3] P. von Ballmoos, Hyperfine Interactions. **228** (2014) 91.
 - [4] J. L. Wang *et al.*, Int. J. Mod. Phys. E **23**, no.12, (2014) 1450088.
 - [5] G. Chen *et al.*, Phys. Rev. C **86** (2012) 054910.
 - [6] S. Ahlen *et al.*, Nucl. Instrum. Meth. A. **350** (1994) 351.
 - [7] M. Casolino *et al.*, Adv. Space Res. **42** (2008) 455.
 - [8] D. E. Dorfan *et al.*, Phys. Rev. Lett. **14** (1965) 995.
 - [9] PHENIX Collab. (J. Adams *et al.*), Phys. Rev. Lett. **94** (2005) 122302.
 - [10] Y. G. Ma *et al.*, Front. Phys. (Beijing) **7**, (2012) 637-646.
 - [11] L. Bergström, AIP Conf. Proc. **478** (1999) 352.
 - [12] S. Zhang *et al.*, Chinese Physics C. **35** (2011) 741.
 - [13] J. Schaffner *et al.*, Phys. Rev. C. **53** (1996) 1416.

- [14] F. Hofmann *et al.*, Phys. Rev. C. **64** (2001) 025804.
- [15] STAR Collab. (B. I. Abelev *et al.*), Science. **328** (2010) 58.
- [16] STAR Collab. (B. I. Abelev *et al.*), Nature. **473** (2011) 353.
- [17] Y. L. Yan *et al.*, Phys. Rev. C, Nucl. Phys. **85** (2012) 024907.
- [18] Y. L. Yan *et al.*, Phys. Rev. C, Nucl. Phys. **81** (2010) 044914.
- [19] B. H. Sa *et al.*, Comput. Phys. Commun. **184**, (2013) 1476-1479.
- [20] G. Chen *et al.*, Phys. Rev. C. **88** (2013) 034908.
- [21] G. Chen *et al.*, J. Phys. G, Nucl. Part. Phys. **41** (2014) 115102.
- [22] T. Sjöstrand *et al.*, J. High Energy Phys. **05** (2006) 026.
- [23] B. L. Combridge *et al.*, Phys. Lett. B. **70** (1977) 234.
- [24] B. H. Sa *et al.*, Comput. Phys. Commun. **90** (1995) 121.
- [25] A. Tai *et al.*, Comput. Phys. Commun. **116** (1999) 353.
- [26] K. Stowe, An Introduction to Thermodynamics and Statistical Mechanics (Cambridge University Press, Cambridge, 2007).
- [27] R. Kubo *et al.*, Statistical Mechanics (North-Holland, Amsterdam, 1965).
- [28] PHENIX Collab. (T. Chujo *et al.*), Eur. Phys. J. C. **49** (2007) 23-28.
- [29] STAR Collab. (G. Agakishiev *et al.*), Phys. Rev. Lett. **108** (2012) 072301.
- [30] Jianhang Zhou. Light (Anti-)Nuclei Production in the STAR Experiment at RHIC, PhD thesis. (2006).
- [31] PHOBOS Collab. (B. Alver *et al.*), Phys. Rev. C. **77** (2008) 061901.